Monitoring of cyclic steam stimulation by inversion of surface tilt measurements

Musa Maharramov[1] and Mark D. Zoback[2]

Abstract

Temperature and pressure changes associated with the cyclic steam stimulation (CSS) used in heavy oil production from sands are accompanied by significant deformation. Inversion of induced reservoir pore-pressure changes from deformation measurements may provide a potentially powerful reservoir-monitoring tool if the issues of measurement noise, uncertainty in model parameterization, and numerical accuracy and stability can be resolved. We discuss inverting injection-induced reservoir pressure changes from observable surface deformations using a linear poroelastostatic model of a heavy oil reservoir. We also present results of inversion from surface tilt measurements taken at a production site undergoing CSS. We demonstrate that a stable inversion of the reservoir pore-pressure change can be achieved from sparse and noisy surface tilt measurements using constrained regularized optimization. The results provide an insight into the heterogeneity of reservoir stimulation and could help with optimizing well locations and stimulation protocols.

Introduction

Surface and subsurface deformation is an important and often easily measurable indicator of production-induced changes in reservoir parameters. The theory of quasi-static poroelastic deformation provides a framework for quantitative assessment of surface and subsurface deformation as a result of pore-pressure changes (Rice and Cleary, 1976; Segall, 1985) and is based on Biot's theory of fluid-infiltrated porous media (Biot, 1941). In this work, we apply the methodology and computational framework of Maharramov (2012), previously applied to pore-pressure inversion in a conventional gas reservoir, to estimating pore-pressure changes from surface tilt measurements at a heavy oil reservoir undergoing cyclic steam stimulation (CSS) described by Walters and Zoback (2013). This method is conceptually similar to the techniques used by Vasco et al. (2000), Du and Olson (2001), and Hodgson et al. (2007) but relies on regularized constrained optimization to address the issues of measurement noise and imposing in situ stress constraints.

CSS is used to reduce the viscosity of heavy oils so that the oil will flow to production wells. This is achieved by injecting high-temperature steam into the formation during an injection period that typically lasts a few weeks or months. This is followed by a "soaking" period during which viscosity of the oil is dramatically reduced due to heat from the steam (Hinkle and Batzle, 2006). Usually, the same wells are used for injection and production. Because oil recovery is dependent on effective injection, it is important to understand and monitor the steam front. This should allow for the appropriate determination of steam paths and the effects of reservoir heterogeneity on steam injection and production.

This work is part of an interdisciplinary study of a heavy oil reservoir undergoing cyclic steam stimulation (Walters and Zoback, 2013). Steam was injected in two cycles, with the first injection in Cycle 1 running from November 2007 through January 2008. Surface tilt measurements were collected from 30 surface tilt stations during Cycle 1 only. No tilt measurements were collected during the following cycle, and this work focuses only on estimating the pore-pressure increase in the reservoir during Cycle 1. Cycle 1 steam injection ran in two overlapping phases: Phase 1 ran from the beginning of the injection through mid-December, and Phase 2 overlapped with Phase 1 and ran through the beginning of January. During Phase 1, steam was injected in the western part of the reservoir, followed by injection in the eastern part in Phase 2. There are 33 production/injection wells as shown in Figure 1 (Walters and Zoback, 2013). Positions of 25 (out of a total of 30) surface tilt stations that were deemed to provide usable data are shown in Figure 2.

Method

We begin by formulating a closed system of equations that describes a quasi-static linear poroelastic medium (Segall, 2010):

$$\frac{\partial}{\partial x_j}\left[\mu\left(\frac{\partial u_i}{\partial x_j}+\frac{\partial u_j}{\partial x_i}\right)+\frac{2\mu\nu}{1-2\nu}\frac{\partial u_l}{\partial x_l}\delta_{ij}\right]=\alpha\frac{\partial p}{\partial x_i}-f_i=0, i,l=1,2,3 \quad (1)$$

and

$$S_\alpha\frac{\partial p}{\partial t}-\frac{\kappa}{\eta}\nabla^2 p=-\alpha\frac{\partial}{\partial t}(\nabla\cdot\mathbf{u}). \quad (2)$$

In the above equations, summation is carried out on repeating indices, u_i, i = 1, 2, 3 are the components of a spatially distributed displacement vector field $\mathbf{u}$; p is the pore-pressure change; f_i is a differential body-force distribution; and μ, ν, α, κ, η, and S_α, are the shear modulus, Poisson's ratio, Biot's coefficient, permeability, fluid viscosity, and storage coefficient, respectively (Wang, 2000; Segall, 2010). Note that the displacement and pore pressure in these equations are relative to a reference state, not the total values. The equilibrium equation 1 and flow equation 2 are fully coupled and are obtained from combining the constitutive laws for a poroelastic medium with quasi-static field equations. The equations are "quasi-static" in the sense that the stress field is assumed to be in a state of static equilibrium, even though changes of the pore pressure in time induce changes of the stress field. We can think of this as a "slow-change" asymptotic approximation, both in time and space. The most mathematically rigorous way of computing the displacement field and associated pore-pressure

[1]Formerly Stanford Exploration Project; presently ExxonMobil Upstream Research Company.
[2]Stanford University.

https://doi.org/10.1190/tle37050350.1.

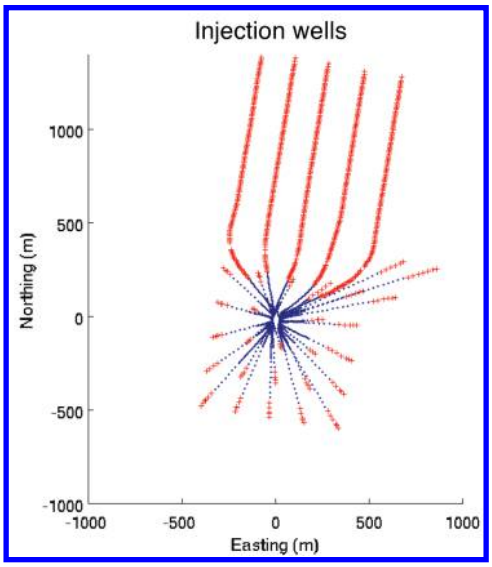

Figure 1. Injection well trajectories. The portions of well trajectories that are within the reservoir are shown in red.

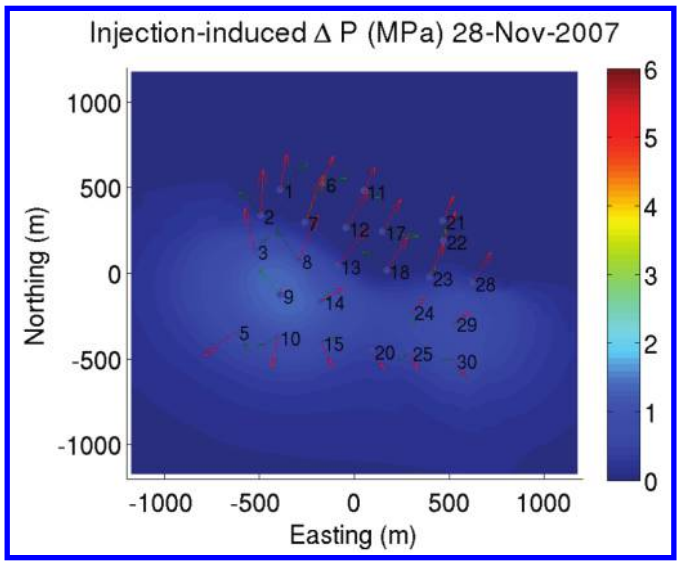

Figure 2. Inverted cumulative pore-pressure change (color scale) and differential tilt measurements (arrows) for $\epsilon = 10^{-3}$ at the beginning of Phase 1 of Cycle 1, after two weeks of injection. The observed differential tilts are shown here and subsequently in green; modeled tilts are in red.

change is to solve a boundary-value problem for equations 1 and 2 with known data (e.g., known pressure evolution within existing wells, measured earth displacements, or estimated stresses) used as boundary or initial conditions. However, even in the simplest case of a homogeneous medium, an analytical solution of boundary-value problems for equations 1 and 2 is challenging. Uncoupling equations 1 and 2, where permissible, could result in more tractable problems, both analytically and numerically. For example, assuming a known pore-pressure change, we can solve the system of equation 1 for the displacement field u_i, using $\alpha\partial p/\partial x_i$ in the right-hand side as a "body-force" distribution (Geertsma, 1973; Segall, 1992). We can use the elastostatic Green's tensor $g_i^k\left(x_1,x_2,x_3;\xi_1,\xi_2,\xi_3\right)$ for the pure elastic equilibrium equation in the left-hand side of equation 1 to compute the displacement u_i due to a pore-pressure change p in a reservoir volume V as

$$u_i = -\alpha\int_V g_i^k \frac{\partial p}{\partial \xi_k} d\xi_1 d\xi_2 d\xi_3 = \alpha\int_V \frac{\partial g_i^k}{\partial \xi_k} p d\xi_1 d\xi_2 d\xi_3 , \quad (3)$$

assuming $f_i = 0$ (including body forces is trivial). The elastostatic tensor $g_i^k\left(x_1,x_2,x_3;\xi_1,\xi_2,\xi_3\right)$ in equation 3 has the meaning of the displacement along axis i at point (x_1, x_2, x_3) due to a concentrated force along axis k at point (ξ_1, ξ_2, ξ_3), and the right-hand side of equation 3 is obtained using integration by parts (Wang, 2000; Segall, 2010). From equation 3, we can see that the divergence of the elastostatic tensor has the meaning of deformation due to a concentrated center of dilatational.

To apply equation 3 to practical reservoir models and computation of surface displacements, the corresponding Green's function should be obtained for a half-space with the free-surface boundary condition imposed on its bounding plane (Segall, 2010). For a homogeneous medium, we can use the analytical expression for the Green's function obtained by Mindlin (1936).

Modeling displacements from pore-pressure change. We can use the operator described by equation 3 for forward modeling the displacement field from a specified pressure change. Note that operator 3 is a nonstationary convolutional integral operator for a homogeneous medium. The convolution is nonstationary due to the presence of $x_3 + \xi_3$ in the elastostatic Green's tensor. Integration along the horizontal axes can be accelerated by applying the operator in the wavenumber domain. However, integration along the vertical axis should still be carried out separately for different values of x_3, so the integration kernel is effectively four-dimensional. Assuming the reservoir to be thin in comparison with its lateral extents, which is widely true in practice, we can replace the vertical integral with a mean value of the integrand times the reservoir thickness:

$$u_i\left(x_1,x_2,x_3\right) = \alpha\int_{\mathrm{Proj}_{(\xi_1,\xi_2)}V} h\left(\xi_1,\xi_2\right)\frac{\partial g_i^k\left(x_1,x_2,x_3;\xi_1,\xi_2,S\right)}{\partial \xi_k} p\left(\xi_1,\xi_2,S\left(\xi_1,\xi_2\right)\right) d\xi_1 d\xi_2 , \quad (4)$$

where $S = S(\xi_1, \xi_2)$ is the middle surface of the reservoir, and $h(\xi_1, \xi_2)$ is the reservoir thickness. For a nonflat reservoir, g_i^k effectively depends not only on differences $x_1 - \xi_1$ and $x_2 - \xi_2$ but on integration variables as well. By modeling subsidence using operators 3 and 4, we are able to fully account for the asymmetric nature of the depletion pattern by using the most general form of Green's tensor for a homogeneous half-space. In that respect, this approach represents an advancement of the purely analytical techniques for axisymmetric reservoirs presented by Geertsma (1973) and Segall et al. (1994), and is similar to the method used by Hodgson et al. (2007).

For mild heterogeneity, when the medium parameters slowly change in space, asymptotic methods can be used to account for the first-order effects of the heterogeneity. However, such an approach is inherently limited to moderate heterogeneity. Lateral heterogeneity of medium parameters is subject to considerable uncertainty, while layered models are of particularly high importance as a dominant stratigraphy. We therefore focus on modeling

displacements for a vertically heterogeneous and horizontally slowly varying medium. Assuming known displacements s_i at a fixed depth $x_3 = z_{\max}$ (for example, zero displacements below the reservoir) and free-surface boundary conditions at $x_3 = 0$, the problem of modeling subsurface displacements is reduced to solving a boundary-value problem for the elastostatic system 1 with the following boundary conditions:

$$\frac{\partial u_i}{\partial x_3}+\frac{\partial u_3}{\partial x_i}+\frac{2\nu}{1-2\nu}\frac{\partial u_l}{\partial x_l}\delta_{i3_{x_3=0}}=0, u_i\left(x_3=z_{\max}\right)=s_i, \tag{5}$$

where indices run from 1 to 3, summation is carried out on index l, and the body-force distribution is zero. For a laterally homogeneous medium — or under the assumption of slowly laterally varying coefficients — equation 1 can be Fourier transformed in x_1, x_2 in an approach similar to propagator matrix methods (Aki and Richards, 1980; Segall, 2010), resulting in a system of ordinary differential equations in depth:

$$\begin{aligned}
&v_j'=v_{3+j}, j=1,2,3,\\
&\left(\mu v_{3+j}\right)'/\mu=\left(k_{3-j}^2+\frac{(2-2\nu)k_j^2}{1-2\nu}\right)v_j+\frac{k_1k_2}{1-2\nu}v_{3-j}+\frac{ik_j}{1-2\nu}v_6+ik_j\frac{\mu'}{\mu}v_3-i\frac{\alpha}{\mu}k_j\hat{p}, j=1,2,\\
&\left(\mu v_6\right)'/\mu=\frac{1-2\nu}{2(1-\nu)}\left[\left(k_1^2+k_2^2\right)v_3+\frac{i}{1-2\nu}\left(k_1v_4+k_2v_5\right)+\frac{2\nu i}{1-2\nu}\frac{\mu'}{\mu}\left(k_1v_1+k_2v_2\right)+\frac{\alpha}{\mu}p'\right]
\end{aligned} \tag{6}$$

where i is the imaginary unity; the differentiation is with respect to $z = x_3$ (depth); k_1, k_2 are the horizontal wavenumbers; $v_{1,2,3}(z)$ are two-dimensional horizontal Fourier transforms of the three displacement components $u_{1,2,3}$ as functions of depth; $v_{4,5,6}(z)$ are the depth derivatives of $v_{1,2,3}(z)$; and $\hat{p}$ is the two-dimensional horizontal Fourier transform of pressure. For simplicity, we assume Poisson's ratio in equation 6 to be constant. The boundary conditions 5 at $z = 0$ and $z = z_{\max}$ are Fourier-transformed in a similar manner. In combination with the Fourier-transformed boundary conditions and after discretization in depth, the above system is reduced to a linear system of $6N_z$ equations for finding $v_l(j\Delta z)$, $l = 1, 2, \ldots, 6, j = 0, \ldots, N_z - 1$ for each wavenumber pair k_1, k_2, where N_z is the number of depth steps and $\Delta z = z_{\max}/N_z$ is the discretization step. Solution of the above system is efficiently parallelized, with each sparse linear system of $6N_z$ equations solved independently. Furthermore, each of the systems is banded and therefore can be solved in a linear time and memory $O(N_z)$ (Trefethen and Bau, 1997). Although depth-varying models are common in geomechanical applications, and the diffusive nature of induced deformation favors slowly varying models, practical applications exist where a strong lateral heterogeneity should be taken into account. The widely accepted approach to tackling such problems consists in applying the finite elements method to the coupled poroelastic system (Kosloff et al., 1980). While finite elements can handle arbitrary spatial heterogeneity, the main disadvantage of this approach is the necessity to solve a potentially very large system of linear equations with a very sparse but generally unstructured matrix.

Estimating pore-pressure change from displacements. Denoting the operator in the right-hand side of equation 3 as $\mathbf{A}$, the problem of recovering the pore-pressure change from specified displacements can be cast as a least-squares minimization problem (Aster et al., 2011):

$$p=\arg\min\left\|\mathbf{A}p-\mathbf{u}\right\|_{L_2}^2. \tag{7}$$

Using operator 3 requires prior knowledge of medium and reservoir parameters, and using Mindlin's analytical expressions for elastostatic Green's tensor assumes homogeneity of the medium. However, by using a gradient-based optimization solver that only requires the application of the modeling operator $\mathbf{A}$ and its adjoint $\mathbf{A}^*$ we obviate the need to use an explicit matrix representation for the operator, and can substitute it with a more computationally intensive deformation modeling operator for a heterogeneous medium, such as the one described by system 6. In practical applications, the problem described by equation 7 is often mixed-determined (Aster et al., 2011), meaning that the deformation data $\mathbf{u}$ cannot be fit exactly due to measurement noise and unaccounted physical effects, and the data are insufficient to uniquely resolve the pressure change p over the entire computational domain — i.e., problem 7 does not have a unique solution. We address the nonuniqueness using Tikhonov regularization (Tikhonov and Arsenin, 1977; Aster et al., 2011) by adding a term penalizing fast pressure oscillations:

$$p=\arg\min\left\|\mathbf{A}p-\mathbf{u}\right\|_{L_2}^2+\epsilon\left\|\Delta p\right\|_{L_2}^2, \tag{8}$$

where Δ is the Laplace operator, and ϵ is an empirically chosen regularization parameter. We assume that the pressure change is always nonnegative and, to avoid hydraulic fracturing, does not exceed the minimum in situ stress (Zoback, 2010). This results in the following inequality constraints on the pressure change:

$$0\le p\le p_{\max}. \tag{9}$$

The problem described by equations 8 and 9 is solved using the augmented Lagrangian method and a smoothed indicator function of the permitted pressure range (Nocedal and Wright, 2006), reducing the constrained optimization problem to a series of unconstrained problems that can be solved using any gradient-based method (Nocedal and Wright, 2006).

Results

Table 1 summarizes the poroelastic medium and reservoir parameters used in our tests. We solved the regularized optimization problems 8 and 9 over a 2 by 2 km computational domain with a 40 m spacing. We used the value of $p_{\max}$ = 7 MPa in the upper constraint 8 based on estimated vertical stress at the

reservoir depth and assuming the minimal stress to be vertical. Continuous tilt measurements from 25 functional tiltmeters (see Figure 2) were available over a 60-day period. These measurements were decimated to 60 daily measurements from each of the 25 tiltmeters and used in independent inversions of daily cumulative pressure changes. Inversion results for different stages of the injection process are shown in Figures 2, 3, 4, 5, 6, and 7. Although there is a considerable uncertainty with regard to the magnitudes of the medium parameters, this uncertainty does not affect the qualitative evolution of the induced pressure change. Figures 2, 3, 4, 5, 6, and 7 show inversion results at various stages of Cycle 1 injection, with the regularization parameter $\epsilon = 10^{-3}$. A maximum cumulative pressure change of 6.1 MPa was achieved on 6 January 2008. Note that the migration of the pressure peak eastward with the progress of injection from Phase 1 to Phase 2 and the lack of significant pressure change at the center of the modeling domain are consistent with the geometry of injection wells in Figure 1. No value of pressure change was prescribed along the boundaries of the computational domain, and the inversion results indicate a significant pressure increase in the

Table 1. The poroelastic medium and reservoir parameters used in the inversion.

Parameter	Value	Units
Shear modulus μ	.34	GPa
Poisson's ratio ν	.25	
Biot's coefficient α	.95	
Average true vertical depth to reservoir	455	meters
Average reservoir thickness	50	meters

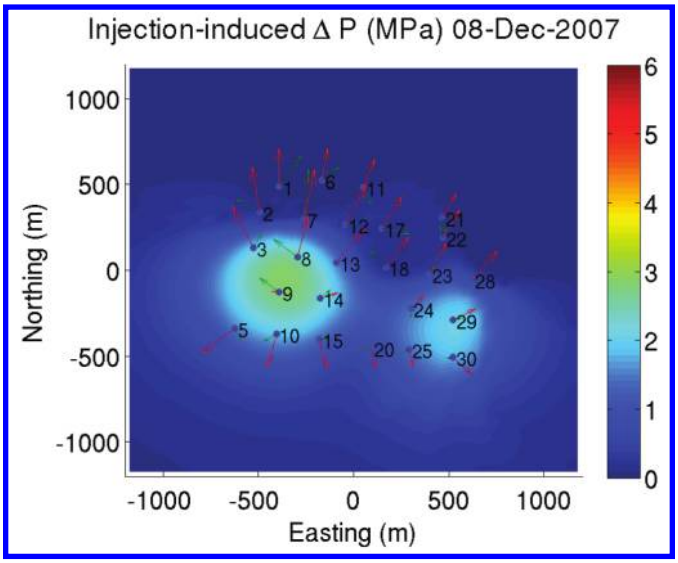

Figure 3. Inverted cumulative pore-pressure change (color scale) and differential tilt measurements (arrows) for $\epsilon = 10^{-3}$ at the end of Phase 1 of Cycle 1, after 24 days of injection.

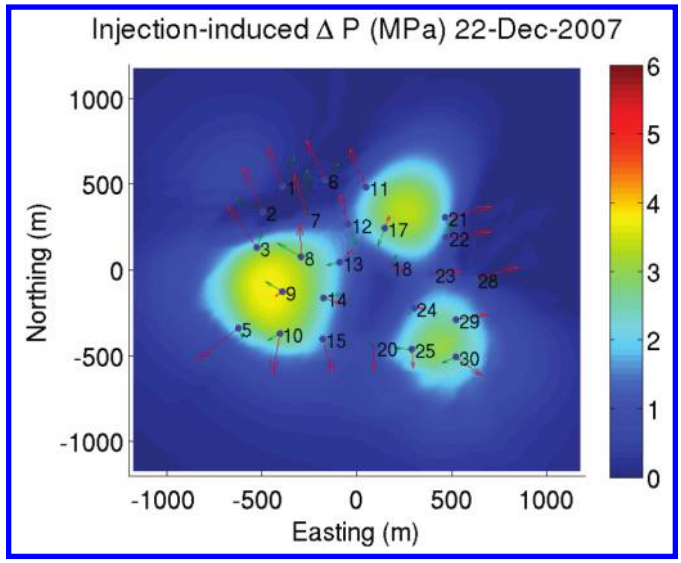

Figure 5. Inverted cumulative pore-pressure change (color scale) and differential tilt measurements (arrows) for $\epsilon = 10^{-3}$, after 38 days of injection.

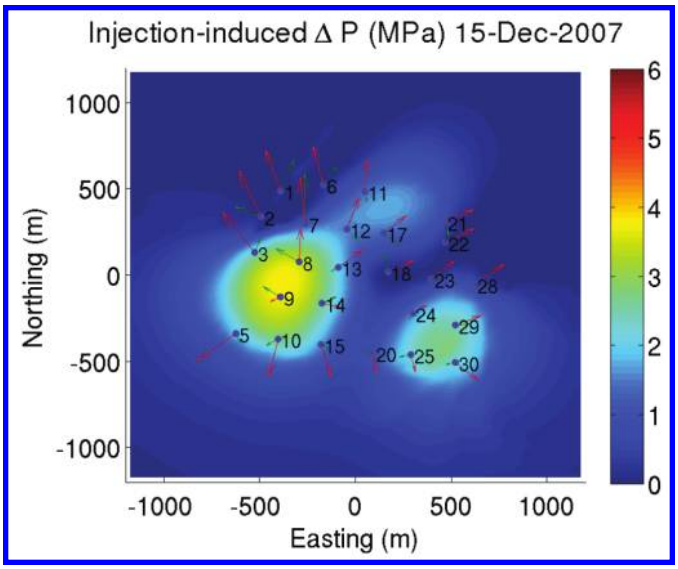

Figure 4. Inverted cumulative pore-pressure change (color scale) and differential tilt measurements (arrows) for $\epsilon = 10^{-3}$ at the beginning of Phase 2 of Cycle 1, after 31 days of injection.

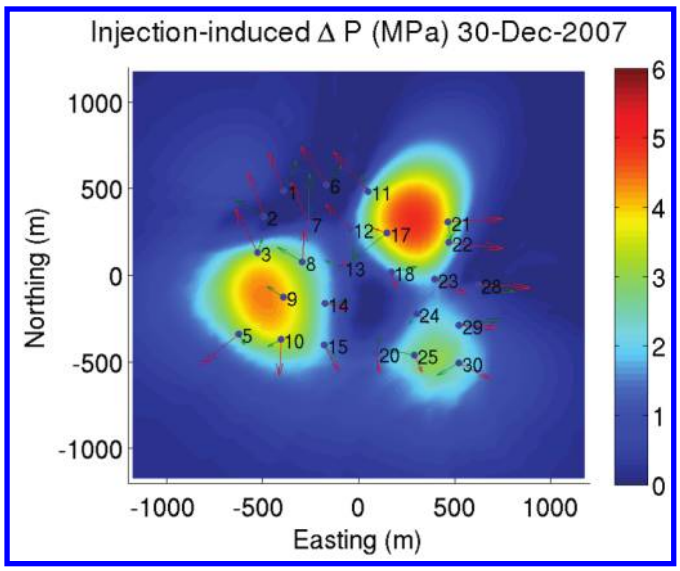

Figure 6. Inverted cumulative pore-pressure change (color scale) and differential tilt measurements (arrows) for $\epsilon = 10^{-3}$ during Phase 2 of Cycle 1. Day 46 of the injection.

eastern part of the modeling domain, consistent with the fact that a considerable fraction of the injection wells are located in that area. Also note that no temporal regularization was used in the inversion — i.e., separate inversions were performed for each set of tilt observations. The fact that the resulting pore-pressure estimates are continuous in time indicates consistency of our input data and stability of the inversion. Regularization of problems 8 and 9 results in a trade-off between data fidelity and smoothness of the inverted pressure change. Choice of regularization parameters in inverse problems is often empirical and can be dictated, for example, by fitting the observed data within a prescribed discrepancy on the data-misfit versus regularization trade-off curve (Aster et al., 2011). However, our primary focus is on understanding the spatial propagation of pressure fronts rather than quantitative accuracy of the inverted pressure change. Given the considerable uncertainty in medium and acquisition parameters, more important than picking a specific value of the regularization parameter ϵ is to ensure the consistency of inversion results for different values of ϵ. We conducted optimization for a wide range of regularization parameters $10^{-3} \le \epsilon \le 10^{-2}$ (Figures 8a–10c). Increasing the value of the regularization parameter has, as expected, a smoothing effect on the inverted pore-pressure change, however, does not change the qualitative picture of pressure front propagation.

Conclusions and perspectives

Injection-induced pore-pressure changes can be stably estimated from surface tilt measurements. While quantitative estimates are affected by the uncertainty in medium and reservoir parameters, the inversion provides a useful insight into the temporal evolution of pressure profiles. Well log data could provide more accurate parameter definition and allow using vertically heterogeneous medium models with equation 6. Scarcity of data and relatively low accuracy of tilt measurements result in highly ill-posed inversion problems that are, however, amenable to regularization and multiscale solution. However, satellite differential radar interferometry has produced maps of surface displacement with subcentimeter-level precision (Zebker et al., 1994), and many of the disadvantages of using tilt measurement data can be remedied by complementing tilt data with differential GPS or InSAR observations (Segall, 2010).

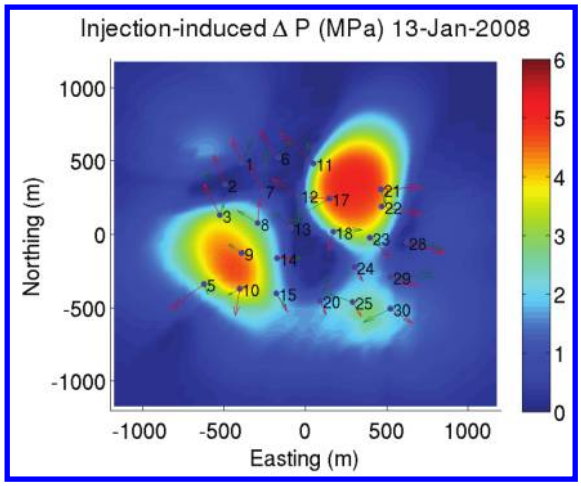

Figure 7. Inverted cumulative pore-pressure change (color scale) and differential tilt measurements (arrows) for $\epsilon = 10^{-3}$ during Phase 2 of Cycle 1. Day 60 of the injection. Note the increase of pressure from Figure 6 to Figure 7 in the northeast of the computational domain. This matches the geometry of injection wells within the reservoir in Figure 1.

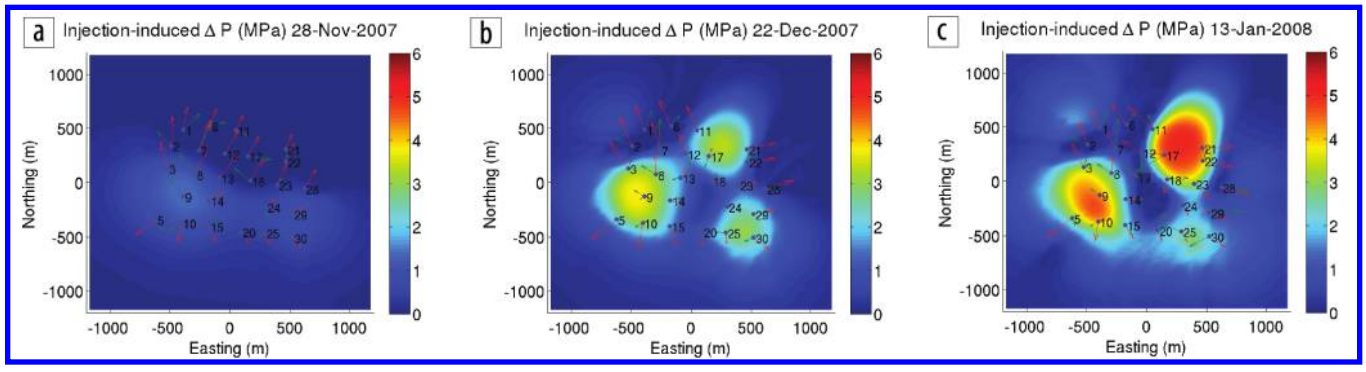

Figure 8. Cumulative pore-pressure change with $\epsilon = 10^{-3}$ (a) 14, (b) 38, and (c) 60 days into the injection cycle.

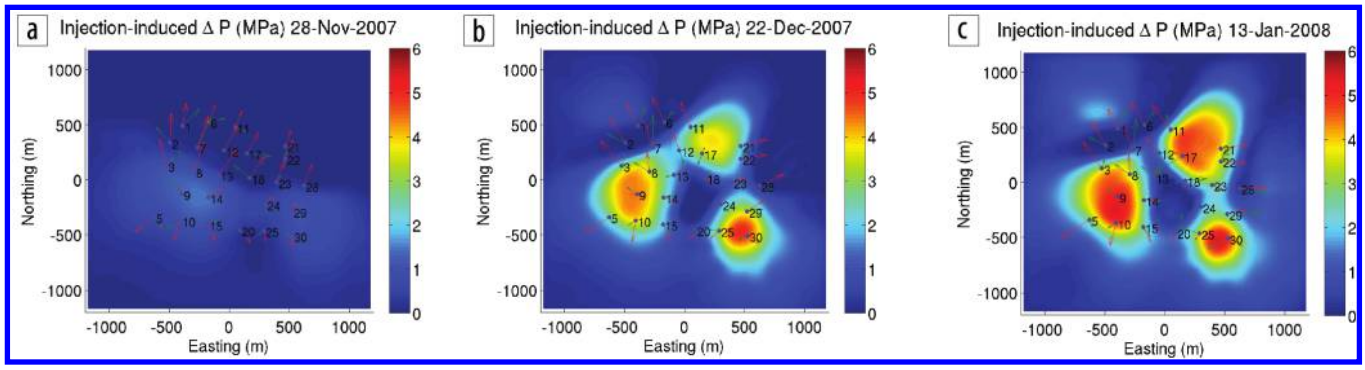

Figure 9. Cumulative pore-pressure change with $\epsilon = 5 \times 10^{-3}$ (a) 14, (b) 38, and (c) 60 days into the injection cycle.

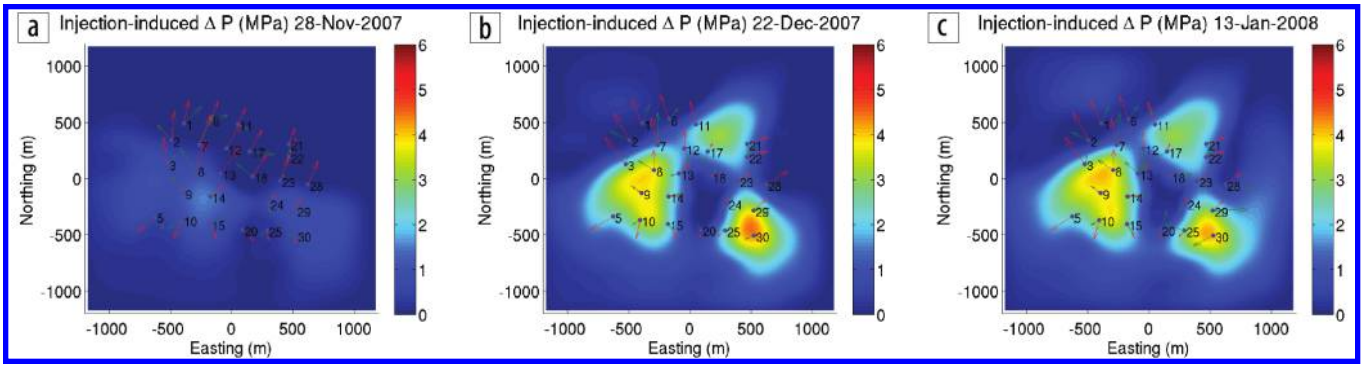

Figure 10. Cumulative pore-pressure change with $\epsilon = 10^{-2}$ (a) 14, (b) 38, and (c) 60 days into the injection cycle.

It should be noted that the extent to which the theory of linear poroelastic deformation can be applied to heavy oil sands is not fully understood. For example, thermal effects may significantly alter heavy oil formations and their poroelastic properties. Furthermore, modeling steam injection in the presence of "wormholes" created as a result of sand production (Hinkle and Batzle, 2006) and preexisting hydraulically conducting faults may require use of techniques similar to modeling fluid-filled chambers that are ubiquitous in volcanology (Segall, 2010). Time-lapse seismic surveys and microsesimic data may provide spatial constraints on the location of activated fluid-filled faults and very high-permeability areas within the reservoir; this information can be used to modify the underlying deformation model. However, the linear poroelastic deformation model, effectively equivalent to modeling reservoir expansion using distributed dilatational sources, appears to be a useful first approximation that can provide at least qualitative insight into the propagation of steam fronts and reservoir heterogeneity. TLE

Acknowledgments

The authors would like to thank Randi Walters, Stewart Levin, Helen Yam, Richard Smith, Mark Meadows, Paul Segall, Ran Bachrach, Douglas Foster, and Yongyi Li for a number of useful discussions and suggestions.

Corresponding author: musa@sep.stanford.edu

References

Aki, K., and P. G. Richards, 1980, Quantitative seismology: Theory and methods: W. H. Freeman.

Aster, R., B. Borchers, and C. H. Thurber, 2011, Parameter estimation and inverse problems: Academic Press.

Biot, M. A., 1941, General theory of three-dimensional consolidation: Journal of Applied Physics, **12**, no. 2, 155–164, https://doi.org/10.1063/1.1712886.

Du, J., and J. E. Olson, 2001, A poroelastic reservoir model for predicting subsidence and mapping subsurface pressure fronts: Journal of Petroleum Science Engineering, **30**, no. 3–4, 181–197, https://doi.org/10.1016/S0920-4105(01)00131-0.

Geertsma, J., 1973, Land subsidence above compacting oil and gas reservoirs: SPE-AIME European Spring Meeting, no. 3730.

Hinkle, A., and M. Batzle, 2006, Heavy oils: A worldwide overview: The Leading Edge, **25**, no. 6, 742–749, https://doi.org/10.1190/1.2210073.

Hodgson N., C. MacBeth, L. Duranti, J. Rickett, and K. Nihei, 2007, Inverting for reservoir pressure change using time-lapse time strain: Application to Genesis Field, Gulf of Mexico: The Leading Edge, **26**, no. 5, 649–652, https://doi.org/10.1190/1.2737104.

Kosloff, D., R. Scott, and J. Scranton, 1980, Finite element simulation of Wilmington oil field subsidence: I. Linear modelling: Tectonophysics, **65**, no. 3–4, 339–368, https://doi.org/10.1016/0040-1951(80)90082-7.

Maharramov, M., 2012, Identifying reservoir depletion patterns with applications to seismic imaging: SEP Report, **147**, 193–218.

Mindlin, R. D., 1936, Force at a point in the interior of a semi-infinite solid: Physics, **7**, no. 5, 195–202, https://doi.org/10.1063/1.1745385.

Nocedal, J., and S. J. Wright, 2006, Numerical optimization: Springer.

Rice, J. R., and M. P. Cleary, 1976, Some basic stress diffusion solutions for fluid-saturated elastic porous media with compressible constituents: Reviews of Geophysics, **14**, no. 2, 227–241, https://doi.org/10.1029/RG014i002p00227.

Segall, P., 1985, Stress and subsidence resulting from subsurface fluid withdrawal in the epicentral region of the 1983 Coalinga earthquake: Journal of Geophysical Research. Solid Earth, **90**, no. B8, 6801–6816, https://doi.org/10.1029/JB090iB08p06801.

Segall, P., 1992, Induced stresses due to fluid extraction from axisymmetric reservoirs: Pure and Applied Geophysics, **139**, no. 3–4, 535–560, https://doi.org/10.1007/BF00879950.

Segall, P., 2010, Earth and volcano deformation: Princeton University Press.

Segall, P., J.-R. Grasso, and A. Mossop, 1994, Poroelastic stressing and induced seismicity near the Lacq gas field, southwestern France: Journal of Geophysical Research, **99**, no. B8, 15,423–15,438, https://doi.org/10.1029/94JB00989.

Tikhonov, A. N., and V. Y. Arsenin, 1977, Solution of ill-posed problems: Winston & Sons.

Trefethen, L. N., and D. Bau, 1997, Numerical linear algebra: SIAM.

Vasco, D. W., K. Karasaki, and C. Doughty, 2000, Using surface deformation to image reservoir dynamics: Geophysics, **65**, no. 1, 132–147, https://doi.org/10.1190/1.1444704.

Walters, R., and M. Zoback, 2013, Microseismicity and surface deformation of a heavy-oil reservoir undergoing cyclic steam stimulation: 83rd Annual International Meeting, SEG, Expanded Abstracts, 2218–2222, https://doi.org/10.1190/segam2013-0431.1.

Wang, H., 2000, Theory of linear poroelasticity with applications to geomechanics and hydrogeology: Princeton University Press.

Zebker, H. A., P. A. Rosen, R. M. Goldstein, A. Gabriel, and C. L. Werner, 1994, On the derivation of coseismic displacement fields using differential radar interferometry: The Landers earthquake: Journal of Geophysical Research, **99**, B10, 19617–19634, https://doi.org/10.1029/94JB01179.

Zoback, M., 2010, Reservoir geomechanics: Cambridge University Press.